J Therm Anal Calorim (2013) 111:1345–1349
DOI 10.1007/s10973-012-2460-x

Synthesis of nanocrystalline zinc manganese oxide by thermal decomposition of new dinuclear manganese(III) precursors

Mohammad Hossein Habibi · Elham Askari

Received: 23 February 2012 / Accepted: 20 April 2012 / Published online: 15 May 2012

Abstract Nanocrystalline manganese-doped zinc oxide was synthesized by thermal decomposition of a zinc oxide sol with two new dinuclear manganese(III) complexes as precursor. Thermal analysis results indicated that the decomposition of manganese precursors occurred at 269 and 314 °C. X-ray structural analysis shows the presence of dimanganese core in the complexes and the binding of the ligands to the manganese(III) is through N_2O_2. The manganese-doped zinc oxide composite was characterized by means of X-ray diffraction, scanning electron microscopy, and UV–Vis spectroscopy. Structural properties of the composites elucidated that the manganese ions have substituted the zinc ions without changing the wurtzite structure of zinc oxide.

Keywords Manganese precursor · Thermal decomposition · Thermal properties · Nanocrystalline · Zinc manganese oxide

Introduction

Zinc oxide (ZnO)-based oxides have n-type semiconducting properties, wide bandgap, and excellent chemical and thermal stability, which makes them potentially useful in solar cells, light-emitting diodes, and thin-film transistor liquid–crystal displays [1–3]. Zinc oxide is a semiconductor with a wide band gap (3.3 eV), which can absorb UV light with the wavelength equal or less than 385 nm. Zinc oxide is used in many applications such as optical coatings, solar cells, electrical devices, and in gas sensors. It is desirable that zinc oxide absorbs not only UV but also visible light. This can be achieved by implanting transition metal ions such as manganese [4–6]. Different methods have been applied to prepare zinc oxide and doped zinc oxide nanoparticles and can be categorized into either chemical or physical methods. The chemical methods for preparation of zinc oxide and doped zinc oxide nanoparticles are thermal hydrolysis techniques and sol–gel method while the physical method are spray pyrolysis and vapor condensation [7]. Band gap of zinc oxide can be narrowed or split into several sub-gaps by implanting transition metal ions to absorb visible light [8]. Doping of transition metals (like manganese) increases the surface defects [9, 10] and it affects the optical and electronic properties and can shift the optical absorption towards the visible region. Differential thermal gravimetry (DTG) and thermogravimetry (TG) are useful to study the modes of thermal decompositions of precursors [11–14]. The objective of this work is to synthesis manganese-doped zinc oxide using new manganese precursors by thermal decomposition. In this paper, for the first time, we examined preparation and characterization of manganese zinc oxide nanocrystals using thermal decomposition of new manganese precursors using sol–gel process. Among all of synthesis methods, the sol–gel process used in this study have the advantages of good homogeneity, ease of composition control, low processing temperature, large area coatings, low equipment cost, and good optical properties.

Experimental

Materials and methods

All solvents and chemicals were purchased from Sigma-Aldrich and used as received, except for the amines which

M. H. Habibi (✉) · E. Askari
Department of Chemistry, University of Isfahan, 81746-73441 Isfahan, Iran
e-mail: habibi@chem.ui.ac.ir; habibi284@gmail.com

were distilled under reduced pressure before use. UV–Vis spectra were recorded on a Varian Cary 500 Scan spectrophotometer. Infrared spectra (KBr pellets) were obtained on a Bruker FT-IR (Tensor 27) spectrophotometer. Thermal gravimetric differential thermal analysis (TG–DTA) measurements were carried using a Mettler TA4000 system. The phase structure of undoped and manganese-doped zinc oxide was identified by a Brucker D8-advance X-ray diffractometer with Cu Kα radiation. The surface morphology and chemical composition of undoped and manganese-doped zinc oxide were studied using scanning electron microscope (SEM) (Philips XL-30 operated at 10 kV of acceleration voltage). The Brunauer-Emmett-Teller (BET) method, using nitrogen adsorption at liquid nitrogen temperature 77 K, was employed to measure total surface area of the photocatalysts.

Synthesis and structural determination of manganese complex

Synthesis of $[Mn(L)(H_2O)]_2(PF_6)_2{\cdot}TZ$, TZ = (5-phenyl-1,3,5-triazine-2,6-diamine) (**1**) as precursor is as followings: To a stirring solution of $Mn(CH_3COO)_2{\cdot}2H_2O$ (0.0662 g, 0.500 mmol) in ethanol (25 mL) was added an equimolar of *N,N′*-Bis(2-hydroxy-5-methoxybenzylidene)-propane-1,2-diamine (0.5 mmol) and 2 mmol of 5-phenyl-1,3,5-triazine-2,6-diamine and the mixture was stirred for 3 h. The pink solution turned dark brown immediately upon the formation of Mn(III) complex, and then 0.500 mmol of NH_4PF_6 was added. A dark brown microcrystalline solid was produced by slow evaporation of ethanol at room temperature. The product was then recrystallized from methanol–propanol (2:1 v/v) and dark brown crystals suitable for X-ray crystallography were obtained. Similar procedure was used for preparation of $[Mn(L)(H_2O)]_2(PF_6)_2$ (**2**) using manganese acetate and ligand. Dark brown crystals of complexes **1** and **2** were mounted with a cryoloop and flash-cooled by cold nitrogen stream. All measurements were made at 193(2) K on a Rigaku RAXIS RAPID imaging plate area detector with graphite monochromated Mo Kα radiation. Absorption corrections were applied by the numerical method [15]. The structure was solved by the direct method using SIR2004 [16] and refined on F^2 with all independent reflections by full-matrix least-square method using SHELXL97 program [17]. The non-hydrogen atoms were refined anisotropically. Hydrogen atoms were introduced at the positions calculated theoretically and treated with riding models.

Synthesis and characterization of nanocrystalline zinc manganese oxide

Undoped zinc oxide sol was prepared using zinc acetate dehydrate (99.99 %), 2-propanol and monoethanolamine

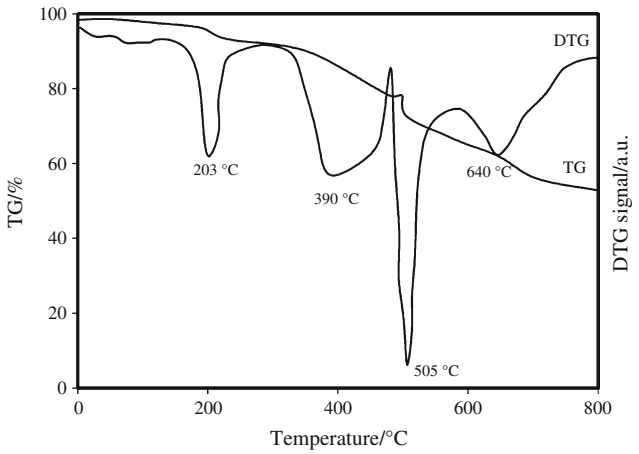

Fig. 1 TG–DTG $[Mn(L)(H_2O)]_2(PF_6)_2{\cdot}TZ$, TZ = (5-phenyl-1,3,5-triazine-2,6-diamine) (**1**)

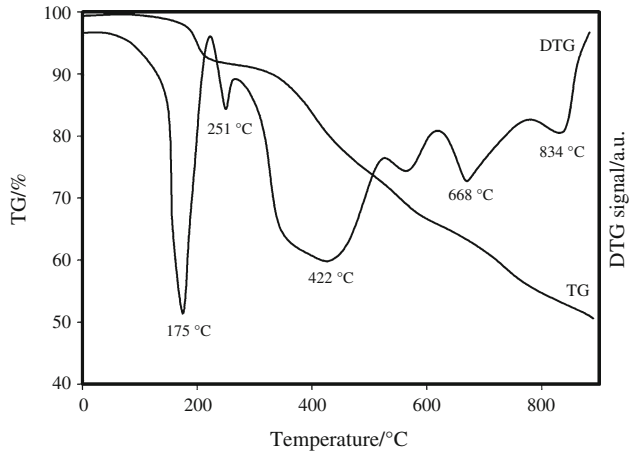

Fig. 2 TG–DTG of $[Mn(L)(H_2O)]_2(PF_6)_2$ (**2**)

Table 1 TG results of manganese complexes

	Temperature/°C	Weight loss/%
Complex **1**	203	7
	390	15
	505	20
	640	5
Complex **2**	175	6
	251	22
	422	16
	668	5

(≥99.0 %) as sol stabilizer. ZnO sol was heated to 60 °C continuously stirred for 1 h to achieve a transparent ZnO sol and then aged for 1 day. Two new dinuclear manganese(III) complexes precursors were used as manganese precursor. It was dissolved in ethanol and acetonitrile as complexing agent which was then added to ZnO sol. The

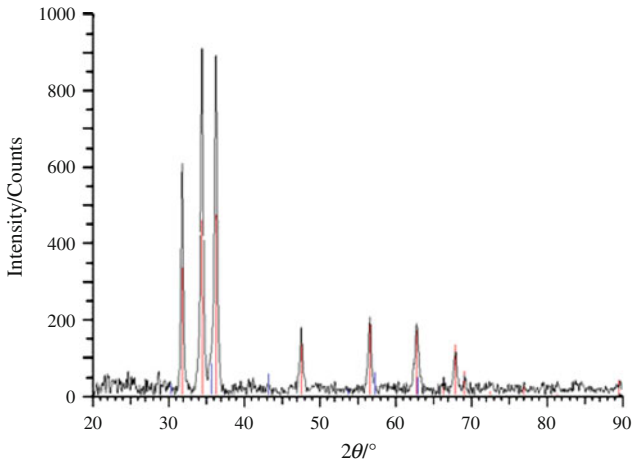

Fig. 3 XRD pattern of manganese-doped zinc oxide

sols were dried at 275 °C for 10 min to evaporate the solvent and remove organic residuals and then were annealed at 350–550 °C for 1 h.

Results and discussion

Synthesis and thermal investigation

Two Mn(III) complexes have been prepared by the reaction of an equimolar of *N,N′*-Bis(2-hydroxy-5-methoxybenzylidene)-propane-1,2-diamine and manganese(II) acetate in the presence of the appropriate axial ligands (water) in aerobic conditions. The air oxidation was continued for a period of 3 h, which resulted in the dark brown color solution. Dark brown crystals of these complexes were obtained in good yield (70–80 %). TG–DTA analysis was conducted to clarify the thermal stability of the two complexes. TG–DTA of **1** and **2** are shown in Figs. 1 and 2, respectively. TG–DTG results in Table 1 indicate that complex **1** shows a major weight loss at 269 °C and complex and **2** shows a major weight loss at 314 °C.

X-ray structural, X-ray diffraction, and SEM analysis

X-ray structural analysis shows the presence of dimanganese core in the complexes with the bond distance of Mn–O (axial) and 2.46; Mn–O (equatorial), 1.89 Å [18]. The electronic spectra of complexes **1** and **2** in methanol and ethanol have two maxima at 238 and 345 nm for **1** and 237 and 360 nm for **2**, respectively. The absorptions at 232 and 238 nm can be related to the spin allowed π–π^* azomethane intraligand transition [19–21]. X-ray diffraction (XRD) diffractogram of the pure zinc oxide and manganese zinc oxide was analyzed to study crystalline aspects. Figure 3 shows the XRD patterns of manganese-doped zinc oxide nanocrystals. The results showed that the samples are highly crystalline with sharp and intense peaks. The XRD peaks indicate the formation of crystalline phase with wurtzite structure of undoped zinc oxide. The XRD patterns of Mn-doped ZnO are similar to pure ZnO. The crystalline size of pure and Mn-doped ZnO can be calculated using Scherrar's formula. The diffraction peaks of the Mn-doped zinc oxide showed a slight shift toward smaller

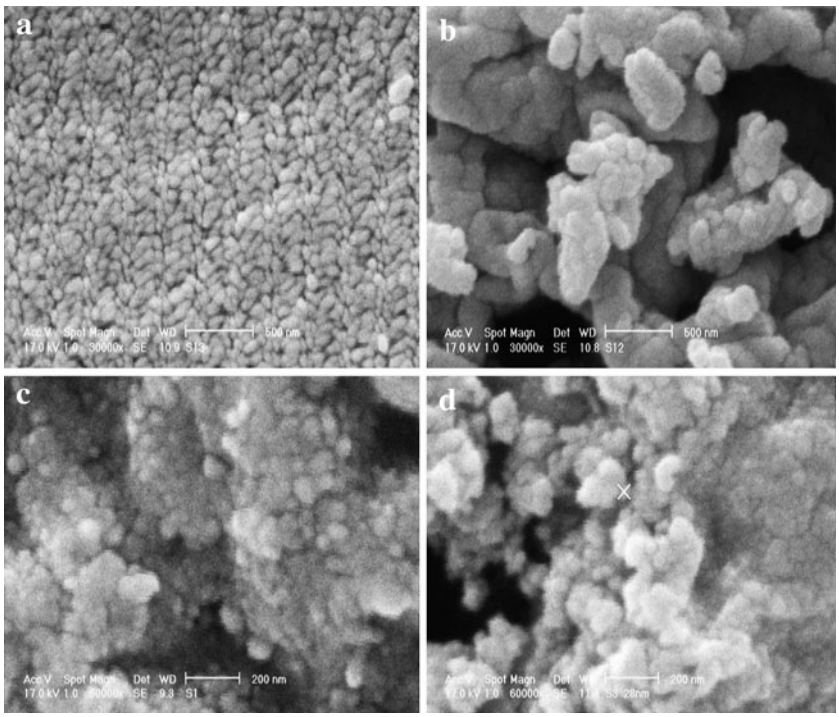

Fig. 4 **a** SEM image of undoped zinc oxide. **b** SEM image of manganese-doped zinc oxide annealed at 350 °C. **c** SEM image of manganese-doped zinc oxide annealed at 450 °C. **d** SEM image of manganese-doped zinc oxide annealed at 550 °C

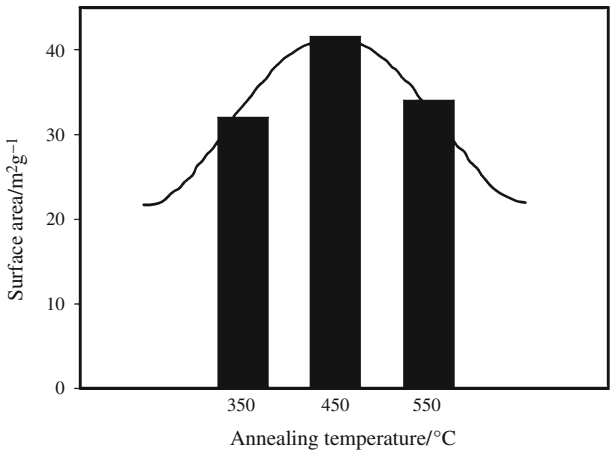

Fig. 5 Effect of annealing temperature on the specific surface area (BET) of manganese-doped zinc oxide

diffraction angle when compared with undoped zinc oxide, indicating that the lattice constants of the manganese-doped zinc oxide changed slightly due to the larger ionic radius of Mn^{2+} (0.83 Å) in comparison with that of Zn^{2+} (0.74 Å). This result shows that manganese-doped zinc oxide has the same wurtzite zinc oxide phase. SEM of undoped and manganese-doped zinc oxide nanocrystals at different stage of annealing (350, 450 and 550 °C) depicting the topography are shown in Fig. 4a, b, c, d, respectively. The surface area of the manganese-doped zinc oxide (Fig. 5) showed the surface area increased when the annealing temperature increases up to 450 °C. However, the surface area was shown to decrease at annealing temperature of 550 °C. Among the four samples, undoped-zinc oxide has the lowest BET surface area (28 m^2g^{-1}), while manganese-doped zinc oxide annealed at 450 °C has the highest BET surface area.

Conclusions

Two new homo binuclear manganese(III) complexes were prepared and characterized as new precursors for manganese-doped zinc oxide. Hexagonal wurtzite-structured manganese-doped zinc oxide nanocrystals were prepared by the thermal decomposition method. Manganese ions were successfully incorporated into lattice sites in the zinc oxide lattice. TG–DTA results indicate that the major weight lose is occured above 250 °C.

Acknowledgements The authors wish to thank the University of Isfahan for financially supporting this work. We would like to thank Yuki Yamane and Takayoshi Suzuki, Department of Chemistry, Faculty of Science, Okayama University, Tsushima-naka 3-1-1, Okayama 700-8530, Japan for X-ray analysis of the two complexes.

References

1. Fang JS, Luo WH, Hsu CH, Yang JC, Tsai TK. The transparent conductive properties of manganese doped zinc oxide films deposited by chemical bath deposition. J Electron Mater. 2012; 41:122–9.
2. Masuda S, Kitamura K, Okumura Y, Miyatake S, Tabata H, Kawai T. Transparent thin film transistors using ZnO as an active channel layer and their electrical properties. J Appl Phys. 2003; 93:71–3.
3. Naghavi N, Rougier A, Marcel C, Guery C, Leriche JB, Tarascon JM. Influence of tin doping on the structural and physical properties of indium–zinc oxides thin films deposited by pulsed laser deposition. Thin Solid Films. 2000;419:160–5.
4. Rekha K, Nirmala M, Nair MG, Anukaliani A. Structural, optical, photocatalytic and antibacterial activity of zinc oxide and manganese doped zinc oxide nanoparticles. Phys B. 2010;405: 3180–5.
5. Sato K, Katayama-Yoshida H. Material design for transparent ferromagnets with ZnO based magnetic semiconductors. J Appl Phys. 2000;39:555–8.
6. Hsiu-Fen L, Shih-Chieh L, Sung-Wei H. The dc thermal plasma synthesis of ZnO nanoparticles for visible light photocatalyst. J Photochem Photobiol A. 2005;174:82–7.
7. Li JH, Shen DZ, Zhang JY, Zhao DX, Li BS, Lu YM, Liu YC, Fan XW. The effect of Mn^{2+} doping on structure and photoluminescence of ZnO nanofilms synthesized by sol–gel method. J Lumin. 2007;122–123:352–4.
8. Sato K, Katayama-Yoshida H. Stabilization of ferromagnetic states by electron doping in Fe, Co or Ni doped ZnO. J Appl Phys. 2001;40:334–6.
9. Ullah R, Dutta JD. Photocatalytic degradation of organic dyes with manganese doped ZnO nanoparticles. J Hazard Mater. 2008;156:194–200.
10. Tam KH, Djurisic AB, Chan CMN, Xi YY, Tse CW, Leung YH, Chan WK, Leung FCC, Au DWT. Antibacterial activity of ZnO nanorods prepared by a hydrothermal method. Thin Solid Films. 2008;516:6167–74.
11. Issa RM, Amer SA, Mansour IA, Abdel-Monsef AI. Thermal studies of bis salicylidene adipic dihydrazone derivatives and their complexes with divalent Ions of Mn, Co, Ni, Cu and Zn. J Therm Anal Calorim. 2007;90:261–7.
12. Habibi MH, Askari E. Thermal and structural studies of zinc zirconate nanoscale composite derived from sol–gel process: the effects of heat-treatment on properties. J Therm Anal Calorim. 2012;. doi:10.1007/s10973-012-2205-x.
13. Ramezanzadeh B, Attar M, Farzam M. Effect of ZnO nanoparticles on the thermal and mechanical properties of epoxy-based nanocomposite. J Therm Anal Calorim. 2011;103:731–9.
14. Baji Z, Lábadi Z, Horváth Z, Fried M, Szentpáli B, Bársony I. Temperature dependent in situ doping of ALD ZnO. J Therm Anal Calorim. 2011;105:93–9.
15. Higashi T. Shape program for absorption. Tokyo: Rigaku Corporation; 2005.
16. Burla MC, Caliandro R, Camalli M, Carrozzini B, Cascarano GL, Caro L, Giacovazzo C, Polidori G, Spagna R. An improved tool for crystal structure determination and refinement. J Appl Crystallogr. 2005;38:381–8.
17. Sheldrich GM. SHELXL97. Germany: University of Gottingen; 1997.
18. Naskar S, Biswas D, Mishr B, Adhikary LR, Falvello T, Soler CH, Chattopadhyay SK. Studies on the relative stabilities of Mn(II) and Mn(III) in complexes with N_4O_2 donor environments: crystal structures of $[Mn(pybzhz)_2]$ and $[Mn(Ophsal)(imzH)_2]ClO_4$. Inorg Chim Acta. 2004;357:4257–64.

19. Hwang FM, Chen HY, Chen PS, Liu CS, Chi YC, Shu CF, Wu FL, Chou PT, Peng SM, Lee GH. Iridium(III) complexes with orthometalated : subtle tuning of emission to the saturated red color. Inorg Chem. 2005;44:1344–53.
20. Baldo MA, Thompson ME, Forest SR. High-efficiency fluorescent organic light-emitting devices using a phosphorescent sensitizer. Nature. 2000;403:750–3.
21. Biswas S, Mitra K, Schwalbe CH, Lucas CR, Chattopadhyay SK, Adhikary B. Synthesis and characterization of some Mn(II) and Mn(III). Inorg Chim Acta. 2005;358:2473–81.